Combustion and Flame 159 (2012) 3493–3501

Contents lists available at SciVerse ScienceDirect

Combustion and Flame

journal homepage: www.elsevier.com/locate/combustflame

Two-line thermometry and H_2O measurement for reactive mixtures in rapid compression machine near 7.6 μm

Apurba Kumar Das [a,b], Mruthunjaya Uddi [c], Chih-Jen Sung [b,*]

[a] Department of Mechanical and Aerospace Engineering, Case Western Reserve University, Cleveland, OH 44106, USA
[b] Department of Mechanical Engineering, University of Connecticut, Storrs, CT 06269, USA
[c] Department of Mechanical and Aerospace Engineering, Princeton University, Princeton, NJ 08544, USA

ARTICLE INFO

Article history:
Received 2 February 2012
Received in revised form 19 June 2012
Accepted 29 June 2012
Available online 10 August 2012

Keywords:
Mid-IR water absorption
Quantum cascade laser
Temperature measurement
H_2O number density measurement
Hydrogen ignition
Rapid compression machine

ABSTRACT

A much desired, direct, *in situ*, diagnostics technique is implemented to measure time variations of temperature and water concentration for a reactive mixture in a rapid compression machine (RCM) using quantum cascade laser absorption spectroscopy near 7.6 μm. The temperature measurements in the RCM are successfully conducted for an end of compression pressure of $P_C \sim 11.5$ bar and an end of compression temperature of $T_C \sim 1022$ K for H_2/O_2/Ar mixtures with (0.5% by mole in the reactive mixture) and without water doping. For all cases investigated, the molar percentages of H_2 and O_2 in the reactive mixture are respectively kept at 3% while the balance is Ar, in order to modulate the extent of post-ignition pressure rise. Absorption lines of water at 1316.55 cm^{-1} and 1316.97 cm^{-1} are used in this study for the measurements. A six-pass setup inside the RCM is implemented for the reactive experiments. For determining the line broadening parameters of water in the range of 1316.4–1317.8 cm^{-1} with H_2 or O_2 as a bath gas, a six-pass, 50.8 mm Herriott cell is used in the calibration experiments. The broadening parameters are measured in the pressure range of 300–650 Torr, while the Herriott cell is heated uniformly to temperatures of 460, 500, and 530 K, respectively. With the measured line broadening parameters of water in the bath gases of interest, the temperature and water concentration histories in the RCM runs are experimentally determined. In addition, the experimental results are compared with the simulations with detailed chemistry. Reasonable agreement is found, thereby demonstrating the utility of this mid-IR absorption spectroscopy in RCM experiments. The uncertainties of the associated measurements of temperature and water concentration are also discussed.

1. Introduction

Laser absorption spectroscopy is a useful tool for non-intrusive measurements of temperature and species time histories. Since its advent, quantum cascade laser (QCL) has been successfully used for absorption spectroscopy by various researchers [1–9] for fast and sensitive measurements. Some of the studies successfully achieved even ppbv levels of measurement accuracy [8,9] for trace components in gas mixtures. Tunable QCL in the mid-IR region poses itself as an attractive option for *in situ* laser measurements due to high absorption coefficients, compactness of the system, and narrow line width (<0.001 cm^{-1}).

Despite its distinct advantages, the usage of QCL in combustion studies has been limited. Vanderover and Oehlschlaeger [10] used a 4.6 μm distributed feedback (DFB)-QCL to measure CO and temperature in a shock tube at near atmospheric pressure conditions. A 5.2 μm continuous wave, external cavity, mode hop free (CW–EC–MHF) QCL was used by Chao et al. [11] to measure NO and H_2O in combustion exhaust gases at atmospheric and sub-atmospheric pressure conditions. In a recent study by Uddi et al. [12], direct non-intrusive temperature measurements for inert mixtures in a rapid compression machine (RCM) were implemented using a tunable CW–EC–MHF QCL in the mid-IR region. Temporal temperature was determined based on the ratio of the rotational–vibrational (rovibrational) absorption lines of H_2O at 1316.55 cm^{-1} to that at 1316.97 cm^{-1} by rapidly scanning through the lines at an effective frequency of 200 Hz. Because of the use of single pass arrangement, the inert mixtures studied in [12] were doped with 2.87% H_2O by mole in order to get sufficient absorption signal. In [12], the temperature measurements in the RCM were successfully conducted for end of compression pressures of $P_C = 10$, 15, and 20 bar and temperatures at the end of compression in the range of $T_C = 1000$–1200 K. In addition, the temperature measurements were found to be within ±5 K of the calculated temperatures using adiabatic core assumption [12]. Furthermore, it was shown in [12]

* Corresponding author. Address: Department of Mechanical Engineering, University of Connecticut, Room 484, United Technologies Engineering Building, Storrs, CT 06269, USA. Fax: +1 860 486 5088.
E-mail address: cjsung@engr.uconn.edu (C.-J. Sung).

0010-2180/$ - see front matter © 2012 The Combustion Institute. Published by Elsevier Inc. All rights reserved.
http://dx.doi.org/10.1016/j.combustflame.2012.06.020

Nomenclature

A	absorbance
c	speed of light (m/s)
E''	lower state energy of the transition line (cm^{-1})
$g_V(v_i - v)$	Voigt line shape function ($1/cm^{-1}$)
h	Plank's constant (J-s)
I_v	transmitted laser intensity at v (W/m^2)
I_{Ov}	incident laser intensity at v (W/m^2)
$K(x,y)$	Voigt function, where $x = \frac{v-v_i}{100c\alpha_D}\sqrt{\ln 2}$ and $y = \frac{\alpha_L}{\alpha_D}\sqrt{\ln 2}$
k_B	Boltzmann constant (J/K)
m	mass of molecules (kg)
N	number density (molecules/cm^3)
n	temperature exponent of collisional line broadening coefficient
L	absorption path length (cm)
P	pressure (bar or Torr)
P_c	pressure at the end of compression (bar)
$Q(T)$	partition function at temperature T
$S^N_{v_i}$	absorption line strength of the line with center frequency v_i per molecule basis ($cm^{-1}/(molecule\ cm^{-2})$)
T	temperature (K)
T_C	temperature at the end of compression (K)
T_0	reference temperature, 296 K
$\alpha(v, P, T)$	absorption cross-section as a function of ν, P, and T (m^2/molecule)
α_D	Doppler half width (cm^{-1})
α_L	Collisional half width (cm^{-1})
γ	Collisional line broadening coefficient ($cm^{-1}\ atm^{-1}$)
γ_0	Collisional line broadening coefficient at reference temperature ($cm^{-1}\ atm^{-1}$)
v	frequency of laser (s^{-1})
v_i	center frequency of absorption line (s^{-1})
$\tilde{v}$	wavenumber (cm^{-1}), defined as v/c
χ_j	mole fraction of species j

that the temporal number density of H_2O can be simultaneously measured in the RCM to an accuracy of 1% using the absolute absorption of the two rovibrational lines.

Recognizing the ubiquitous presence of H_2O in most of the common combustion system, this investigation extends the effort of [12] by exploring the use of QCL for much desired, direct, non-intrusive, measurements of temperature and species evolution histories in an RCM for reactive mixtures. Water absorption lines near 7.6 μm are used for determining the temperature history using the two-line ratio method discussed in [12]. Reactive mixtures of H_2/O_2/Ar with and without H_2O doping are studied herein. The absorption length inside the RCM is increased from the previous study [12] by allowing a six-pass arrangement to enhance sensitivity. Previously, Farooq et al. [13] conducted similar measurements of H_2O and temperature in an atmospheric pressure flat flame using a distributed feedback (DFB) diode laser near 2.5 μm. In the present study, a high power tunable QCL at 7.6 μm is used due to its wide tunability and potential of enabling measurements for other species.

It is further noted that the chosen lines broaden and merge at high pressures typical of RCM operating conditions. In addition, the individual merging lines have different broadening coefficients and temperature exponents depending on the buffer gas. Therefore, absorbance calculations using the HITRAN/HITEMP database [14] (the combined database referred to as simply HITRAN hereafter) with appropriate line broadening parameters is required for determining the temperature. Since HITRAN has data only for air broadening [14] and since Ar, H_2, and O_2 are used in the current combustible mixtures, it is important to measure the broadening coefficients of H_2O in these bath gases before the measurements of water concentration and temperature in the RCM experiments can be quantified. In our previous study [12], line by line broadening coefficient (γ) of H_2O by Ar bath gas and its temperature exponent 'n' for the HITRAN database were determined experimentally in the wavelength range of 1316.4–1317.8 cm^{-1}. Following the same procedure and methodology as [12], the broadening parameters (both γ and n) of the same H_2O lines are experimentally determined in this study with either H_2 or O_2 as a bath gas, which will be detailed in due course.

2. Theory of absorption spectroscopy

The theory of absorption spectroscopy is widely available and also explained in [12], and hence is mentioned here in brief for completeness. The fractional transmission of electromagnetic radiation through a uniform medium with a line of sight length L is given by the Beer's law equation:

$$\frac{I_v}{I_{0v}} = e^{-\alpha(v,P,T)NL} = e^{-\sum_i S^N_{v_i}(T) g_V(v_i - v) NL} \tag{1}$$

Here, 'i' denotes the various absorption lines with center frequency v_i that can have absorption at the laser frequency v due to line broadening, $[\alpha(v, P, T)NL]$ is the absorbance, and N is the number density of the absorbing species. The absorption cross-section $\alpha(v, P, T)$ is product of the line strength $S^N_{v_i}(T)$ and the line shape function $g_V(v_i - v)$ approximated by a Voigt profile. Therefore, the ratio of the absorbance of two neighboring lines with center frequencies v_1 and v_2 is given by Eq. (2):

$$\frac{\ln\left(\frac{I_{v_1}}{I_{0v_1}}\right)}{\ln\left(\frac{I_{v_2}}{I_{0v_2}}\right)} = \frac{S^N_{v_1}(T) g_V(v_1)}{S^N_{v_2}(T) g_V(v_2)} \tag{2}$$

In this study, a normalized modeled absorption profile using HITRAN is least square fitted to the normalized experimental absorption profile for determining the temperature. As such, the ratio of peaks from the modeled profile is the criterion for determining the temperature, while the least square fitting ensures that the normalized absorption profiles modeled using HITRAN matches well with the ones obtained from experiments. Also note that at elevated temperatures and pressures typical to RCM operating conditions, each peak can be a merger of multiple lines.

The absorption profile at different conditions of temperature and pressure can be modeled using the data from HITRAN [14]. Reference line strength $S^N_{v_i}(T_0)$ at reference temperature T_0 = 296 K, from HITRAN [14], can be used to determine the line strength $S^N_{v_i}(T)$ at any temperature T using Eq. (3):

$$S^N_{v_i}(T) = S^N_{v_i}(T_0)\frac{Q(T_0)}{Q(T)} e^{\frac{-hcE''}{k_B}\left(\frac{1}{T}-\frac{1}{T_0}\right)} \frac{\left[1 - e^{\left(\frac{-hcv_i}{k_B T}\right)}\right]}{\left[1 - e^{\left(\frac{-hcv_i}{k_B T_0}\right)}\right]} \tag{3}$$

In Eq. (3), E'' is the lower state energy of the transition line centered around v_i, h is the Plank's constant, c is the speed of light, k_B is the Boltzmann constant, and Q is the partition function. The partition function at temperature T, $Q(T)$, is obtained using the latest version

of the partition function code (TIPS_2011.for) originally presented by Fischer et al. [15].

As mentioned earlier, the line shape function $g_V(v_i - v)$ is approximated with a Voigt profile presented by Eq. (4):

$$g_V(v_i - v) = \frac{1}{\alpha_D}\sqrt{\frac{\ln 2}{\pi}}K(x,y) \tag{4}$$

It is noted that in Eq. (1) v denotes any frequency at which the line shape contribution due to absorption line with center frequency v_i is computed. In Eq. (4), the Voigt function is given by

$$K(x,y) = \frac{y}{\pi}\int_{-\infty}^{\infty}\frac{e^{-t^2}}{y^2 + (x-t)^2}dt, \quad \text{where } y = \frac{\alpha_L}{\alpha_D}\sqrt{\ln 2} \text{ and } x = \frac{v - v_i}{100c\alpha_D}\sqrt{\ln 2} \tag{5}$$

The Doppler half width α_D and the collisional half width α_L for each line 'i' are respectively given by

$$\alpha_D = \frac{v_i}{100c^2}\sqrt{\frac{2k_BT\ln 2}{m}} \text{ and } \alpha_L = P\sum_j \gamma_{0_j}\chi_j\left(\frac{T_0}{T}\right)^{n_j} \tag{6}$$

where m is the mass of absorbing molecule, the summation 'j' is over all the bath gas species with mole fractions χ_j, γ_{0_j} is the collisional line broadening coefficient at reference temperature for the bath gas 'j', and n_j is the temperature exponent for the bath gas 'j'. The broadening parameters used in this study for the selected lines are experimentally determined for O_2 and H_2, while the broadening parameters for Ar are taken from our previous study [12]. However, it is expected that the broadening by Ar will dominate, considering relative abundance of Ar compared to the other constituents.

3. Experiments

The experimental setup is described in detail in [12], and the schematic of the experimental setup is shown in Fig. 1. The QCL used here has a wide tunability range (1302–1362 cm^{-1}), high power (100–220 mW), and narrow line width (<0.001 cm^{-1}). Generally, the lead-salt diode lasers found in this wavelength range have low power and require cryogenic cooling, thus making them less desirable for the type of measurements we are interested in. The same setup of six-pass calibration cell used in [12] is employed for the measurements of collisional broadening parameters. This multi-pass setup has also been incorporated in the RCM reaction chamber for more sensitive *in situ* measurements of temperature and water concentration.

An introduction to the rapid compression machine (RCM) used in this study can be found elsewhere [16]. It is a newly built RCM similar to the one in use at our facility but with wider compression ratio range, capable of attaining higher compressed pressure, and other operational improvements. General details of its predecessor can be found in [17,18]. Mittal and Sung [18] demonstrated that an optimized creviced piston geometry in the RCM can improve the temperature uniformity substantially, thereby providing a well-controlled environment for combustion study at low-to-intermediate temperatures and high pressures. Typical RCM studies involve direct measurement of ignition delay from the pressure trace. Additional sampling studies or/and the mid-IR absorption spectroscopy demonstrated in this work can also be conducted to understand the evolution profiles of different important species. Such RCM studies not only provide insight into the ignition behavior of various fuels, but also provides benchmark database for validating chemical kinetic mechanisms to be further reduced and used in predictive modeling.

The laser beam from the QCL is split into two beams using a 50% beam splitter. One of the beams passes through a 3" Ge etalon and is incident on a mercury–cadmium–telluride (MCT) detector (Vigo PVM-2TE-10.6), labeled as Detector 1 in Fig. 1. The scan rate is determined from the peaks of the etalon signal recorded by this detector. A cubic spline fitted through the peak intensities is used as reference for laser energy for the particular scan and later used for minor corrections in the beam intensities used in calculations, which will be discussed in Section 3.1. The other laser beam is directed using mirrors, through two irises which serve as guide for the multi-pass arrangement. The position of the two guiding irises is determined beforehand by aligning for the multi-pass

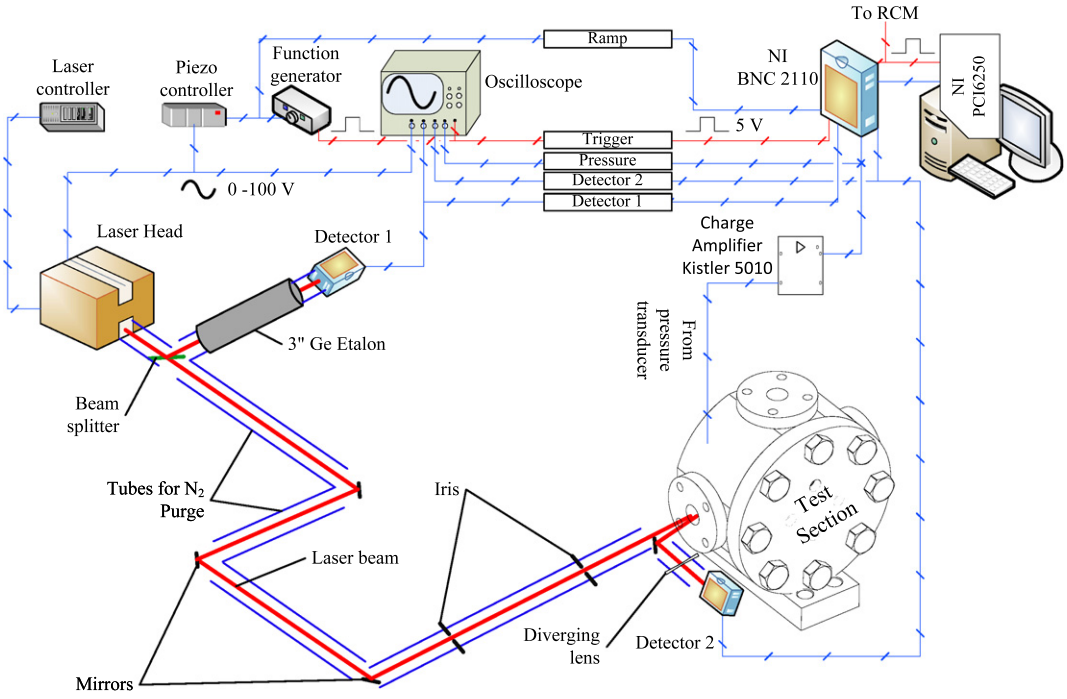

Fig. 1. Schematic of the experimental setup.

arrangement, using a visible red diode laser. The beam then goes through the hole in one of the internal mirrors of the RCM or the calibration cell making multiple passes internally and comes out through the same hole. The mirrors are of focal length 50 mm and are separated by 2″, which is the bore diameter of the RCM. The transmitted beam goes through a diverging lens (−15 mm) before being incident on another MCT detector, labeled as Detector 2 in Fig. 1. The diverging lens is used to immerse the detector in a uniform laser energy flux. The absorption length of a single pass in the RCM is 50.8 mm. The detector signals are recorded both by an oscilloscope and a National Instruments DAQ card. In order to avoid atmospheric water absorption outside the test section, the laser beam is passed through 0.5'' tubes which are purged by pure N_2.

A function generator (BK Precision 4079) connected to a piezo controller (Thorlabs MDT694A) is used to drive the piezo on the laser head and ramp it through the rovibrational lines within ~2 cm^{-1}. The applied voltage on the laser head is a 0–100 V peak-to-peak sine wave at 100 Hz. The laser ramps through the wavelength range twice in each cycle: once while ramping up and another while ramping down. Therefore, the sine wave effectively scans through the wavelength range at 200 Hz.

High purity argon (99.999%, H_2O <1 ppm, total hydrocarbon <0.5 ppm), hydrogen (99.999%, H_2O <2 ppm, total hydrocarbon <0.5 ppm), oxygen (99.994%, H_2O <2 ppm, total hydrocarbon <0.5 ppm), and deionized water (total dissolved solids <0.3571 ppm and electrical resistivity >14 MΩ cm) are used for this study.

3.1. Scan rate and reference signal

As described earlier, one branch of the laser is sent through a 3″ Ge etalon and is detected using Detector 1. The laser signal obtained from Detector 1 is used to derive the laser scan rate and the reference laser energy. Figure 2 shows the Detector 1 laser signal through the etalon. As the peaks of the etalon are separated by a free spectral range (FSR), the instantaneous scan rate can be determined. A smooth polynomial fit to the experimental scan rate is used to transform from time domain to wavenumber domain. The experimental scan rate, the smooth polynomial fit, and the voltage ramp for a typical scan is shown in Fig. 3a. The reference for the laser intensity is determined by a cubic spline fit to the peaks of the etalon. Figure 3b shows the reference laser intensities for two such scans. It is seen that although run to run variations are small, it is still needed to be accounted for when determining the fractional transmission of laser radiation through the test section. In each experiment, a scan with absorption in the test section and the corresponding scan without absorption in the test section are separately taken. Based on the two reference laser intensities from Detector 1, the signal level in Detector 2 for the scan without absorption in the test section is multiplied by the ratio of Detector 1 signals with and without absorption for each time step to obtain the I_0 used for calculating the absorbance.

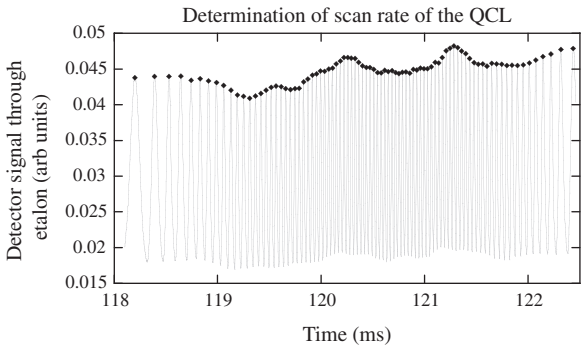

Fig. 2. Transmitted signal through the etalon with sinusoidal voltage ramp (0–100 V) applied to piezo of the laser. The etalon peaks are marked by filled symbols.

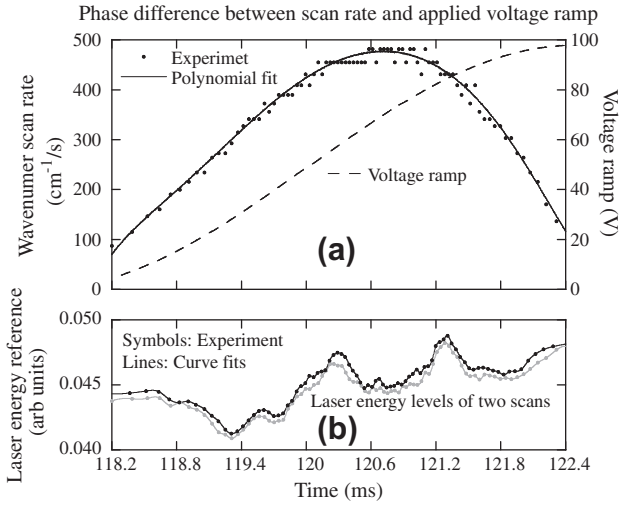

Fig. 3. (a) Scan rate of laser with a sinusoidal voltage ramp (0–100 V) applied to piezo of the laser, showing the phase difference. (b) Laser energy reference from Detector 1 signal for two runs derived from the etalon peaks.

3.2. Calibration in the test cell

The calibration experiments are done similar to the previous study [12]. The multi-pass test cell is used to find line broadening parameters of water absorption lines in the range of 1316.4–1317.8 cm^{-1} for H_2 and O_2 as a bath gas. A six-pass custom built 50.8 mm Herriott cell [19] insulated and heated uniformly to temperatures of 460, 500, and 530 K, in the total pressure range of 300–650 Torr, is used for this purpose. The Herriott cell is arranged in such a way that the laser beam enters and exits through the same hole in one of the mirrors and the total absorption path length is 306 mm. Details regarding determination of the path length inside the multi-pass cell and the temperature characterization of the test cell can be found in our previous study [12]. The uncertainty in determining the path length is estimated to be within ±1 mm.

Water is manometrically added to start, with partial pressures ranging from 3 to 20 Torr. High purity H_2 or O_2 buffer gas is then added to various total pressures in the range of 300–650 Torr. The reference laser beam passing through the etalon is used to determine the line width. The line by line pressure dependence through the H_2 or O_2 broadened half width (γ_0) and temperature dependence of the broadening through the exponent '*n*' for the HITRAN database are extracted through these experiments, as listed in Table 1. More details of these results are explained in Section 5.1.

3.3. RCM experiments

The same multi-pass arrangement as in the calibration test cell is implemented in the RCM to measure the temperature evolution in the reactive mixture. The QCL ramps through the two peaks chosen, which are separated by ~0.6 cm^{-1}, in ~1 ms (details can be found in [12]). A trigger signal generated by LabView simultaneously triggers the function generator for generation of a burst of sine waves applied through the piezo-driver to the laser head, a solenoid to run the RCM, and an oscilloscope for data acquisition. The signals from the two detectors, the voltage ramp, and the test

Table 1
Measured H_2O collisional line broadening parameters in Ar, H_2, and O_2.

Line center $\tilde{\nu}$	Collisional broadening parameters as per $\gamma(T) = \gamma_0(\frac{T_0}{T})^n; T_0 = 296$ K					
	H_2O in argon [12]		H_2O in hydrogen		H_2O in oxygen	
	γ_0	n	γ_0	n	γ_0	n
1316.5408	7.67×10^{-3}	1.99×10^{-3}	0.0679	1.17	0.0149	0.45
1316.5500	8.49×10^{-3}	2.20×10^{-3}	0.0752	1.17	0.0165	0.45
1316.9724	1.07×10^{-2}	5.48×10^{-3}	0.0545	0.73	0.0272	0.55
1317.6105	4.51×10^{-3}	-1.74×10^{-3}	0.0229	−0.29	0.0046	−0.24
1317.6157	8.95×10^{-3}	-3.46×10^{-3}	0.0452	−0.29	0.0091	−0.24

Units: $\tilde{\nu}$ (cm^{-1}); γ_0 (cm^{-1} atm^{-1}).

section pressure transducer voltage are recorded. If needed, the delay between the initiation of laser ramping and the start of RCM compression can be varied to completely map the temperature profile for different repeatable RCM runs.

It is to be noted that the laser and the optical elements are mechanically isolated completely from the RCM bench to avoid any vibration of the same. The RCM used in this study has minor vibrations due to good weight distribution. The effect of RCM vibrations is further eliminated by allowing the laser through a large (3.3 mm) aperture in the mirror. As a result, the inert experiments without absorption and the reactive experiments with absorption are repeatable. Furthermore, the detector active area is 1 mm × 1 mm, and the distance from the aperture in the mirror to the detector active area is 9–10 cm. The solid angle subtended by any point on the aperture to the detector surface is very less (1.59×10^{-5} sr). Therefore, the effect of radiation from hot gases is expected to be insignificant on the detector signal due to this arrangement. Additionally, the emission due to combustion is expected to occur during and after hot ignition. The measurements done in this study are till just before the sharp pressure rise (hot ignition). As such, we expect that the present measurements should be free from any such emission effects.

For each condition, at first the test section is filled with inert mixture without any H_2O and a set of data is acquired to obtain the baseline laser intensity '$I_{0\nu}$' as discussed in Section 3.1. During the reactive run, the Detector 2 signal gives the transmission through the reaction chamber 'I_ν'. The absorbance at high pressures at a particular laser frequency ν, where many absorption lines with center frequencies ν_i can interfere, is calculated as:

$$A_\nu = -\ln\left(\frac{I_\nu}{I_{0\nu}}\right) = NL\sum_i S^N_{\nu_i}(T) g_V(\nu_i - \nu) \tag{7}$$

The temperature is determined, as delineated in Section 2, for reactive mixtures of high purity argon with 3% (by mole) H_2 and 3% O_2, with (0.5%) and without (0%) H_2O doping. RCM measurements are conducted for end of compression pressure of $P_C \sim 11.5$ bar and end of compression temperature of $T_C \sim 1022$ K. The compression ratio employed is 10.3, with 7″ stroke and 0.754″ clearance. According to the method to be described in Section 4, RCM simulations are done using the SENKIN [20] code along with the detailed mechanism of Hong et al. [21]. The experimentally determined temperatures and water concentrations are also compared with the simulated results.

It is also noted that the current mid-IR absorption spectroscopy setup uses CaF_2 windows with high transmittivity in the chosen laser wavelength range. However, CaF_2 windows are very brittle and sudden pressurization stemming from strong ignition can lead to its failure, especially high concentration of H_2/O_2 mixtures in argon would generally ignite violently leading to large pressure spikes. In order to avoid such situation, as a first attempt to demonstrate the underlying method using the present setup, a dilute mixture of H_2/O_2 in argon (as mentioned above) is used for this study.

4. RCM simulation

Simulations of the RCM experiments are carried out using the SENKIN [20] code in conjunction with the CHEMKIN [22] suite. Following the approach detailed in [16,17], the heat loss effects during the compression stroke and after the end of comparison are taken into account in simulations. Non-reactive pressure trace is obtained for each condition using the corresponding mixtures prepared by replacing O_2 with N_2. The pressure trace for the non-reactive run is then used to determine and tabulate the volume as a function of time based on the adiabatic core assumption [16]. This time variation of volume describes the compression stroke and accounts for the heat loss effect during compression as well as the post compression event. In this study, an improved H_2/O_2 mechanism recently reported by Hong et al. [21] is employed to simulate the RCM experiments.

5. Results and discussion

5.1. Calibration experiments

The present calibration setup was validated in our previous study [12]. Moreover, the line strength of water absorption lines in the range of 1316.4–1317.8 cm^{-1} and the line broadening parameters for the same in argon have been experimentally determined [12]. In this study, calibration experiments for determining the line broadening parameters for water absorption lines within 1316.4–1317.8 cm^{-1} are conducted using hydrogen and oxygen as a bath gas, as the information of broadening parameters for these lines is very limited in the literature. Line widths of water absorption lines are determined in the pressure range of 300–650 Torr and at three different temperature conditions of 460, 500, and 530 K. The parameters, γ_0 (the γ value at 296 K) and n, are obtained through a fit to the measured values of γ at various temperature conditions. The broadening parameters for water line broadening in hydrogen and oxygen determined from this study, along with the line broadening parameters in argon from the previous study [12], are listed in Table 1. In a study determining γ_0 of water absorption lines in O_2, Toth and Brown [23] reported the γ_0 value for the line at 1316.97 cm^{-1} to be 0.0306 cm^{-1}/atm which agrees reasonably with 0.0272 cm^{-1}/atm found from this study. However, the γ_0 value of the combined double lines near 1317.61 cm^{-1} was reported to be 0.0065 cm^{-1}/atm in the same study [23], which is almost half of the value determined in this study. Since the strength of the transition near 1317.61 cm^{-1} at room temperature is weak, an independent investigation is required to resolve the observed discrepancy. Nevertheless, the double lines near 1317.61 cm^{-1} are not selected for the current RCM measurements and their effect on our target absorption lines is negligible.

Further, the broadening coefficient for H_2O transition in H_2 bath gas near 1316.97 cm^{-1} was listed as 0.0527 cm^{-1} (at 299 K),

measured by Brown and Plymate [24], which agrees quite well with the measurement in this study. It is to be noted that the value of temperature exponent n changes widely for various H_2O transition lines chosen for this study, especially in H_2 bath gas. For the values listed in the latest version of HITRAN [14], the values of n for H_2O transitions in air within 1316.4–1317.8 cm^{-1} vary from 0.37 to −0.13, while for a wider range in this band (1312.0–1325.0 cm^{-1}), the values of n range from 0.78 to −0.56. Previous studies [25] in different wavelength ranges have shown higher values of n in O_2 or H_2 bath gases when compared to nitrogen (main constituent of air). It was also found that the variation in temperature exponent n of H_2O transition lines is much more in H_2 as compared to nitrogen or O_2 [26].

The combination of the lines at 1316.55 cm^{-1} and 1316.97 cm^{-1} is used for the temperature measurements by fitting with the HITRAN simulation using the updated line broadening parameters in Table 1. Effect of broadening by any intermediate species is considered to be negligible due to very low concentration.

5.2. RCM temperature and water concentration measurements

The transmitted signal I_v is taken as the laser signal from Detector 2 for the reactive run, while the laser baseline signal I_{v0} is taken from the inert run without water and based on the Detector 2 signal after appropriate adjustment as delineated in Section 3.1. As such, the absorbance of the selected lines can be determined from the experimental data. The time to wavenumber domain transformation is done using the laser scan rate information obtained from the Detector 1 signal. The updated broadening parameters determined for different bath gases mentioned in Section 5.1 in conjunction with the HITRAN database are used to model the absorbance profile. The ratio of peak heights is the criterion for determining the temperature. It is worthy to note that apart from the peak heights, the experimental absorbance profiles for the conditions investigated are also matched well with the calculated HITRAN absorbance profiles.

Figures 4 and 5 compare the experimental and simulated time-varying profiles of pressure, temperature, and water mole percentage for the RCM run with water doping, while Figs. 6 and 7 compare the same for the case without water doping. It is noted that the evolution history is time shifted to align the end of compression with time zero. The RCM simulations show good agreement of ignition delay prediction with the experiment, as seen from the comparison of pressure traces in Fig. 4 (with H_2O addition) and 6 (without H_2O doping). However, the peak pressure after ignition is lower for the experiments when compared to the simulations due to heat loss, which is expected.

The comparison between the experimentally determined temperatures and water mole percentages with the RCM simulations for the mixture with H_2O doping is shown in Fig. 5. It is found that the simulated data are within ±5 K of the experimentally determined temperatures for most of the induction time period. The temperature difference becomes more just before ignition at 44.1 ms, beyond which the experimental and simulated pressure traces start to deviate as shown in Fig. 4. An uncertainty analysis for the present temperature determination will be described in Section 5.4. The mole percentage of water determined from the absolute value of the absorbance peak heights confirms 0.5% water

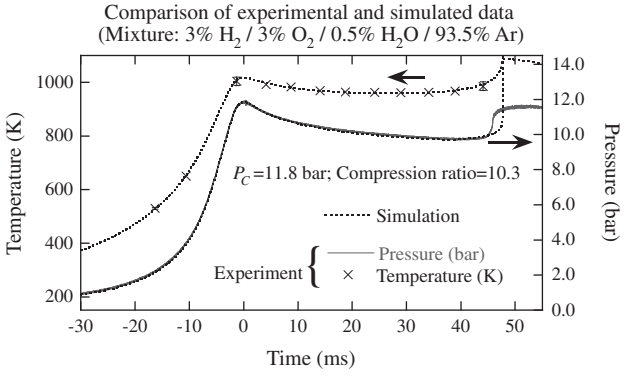

Fig. 4. Comparison of experimental pressure trace and temperature history with simulation for the reactive mixture with 0.5% (by mole) H_2O doping.

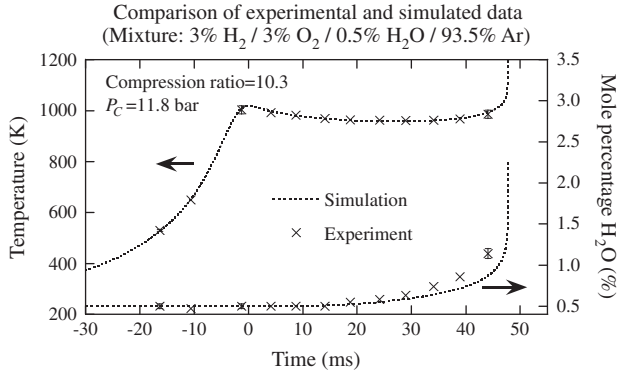

Fig. 5. Comparison of experimentally determined temperatures and water mole percentages with simulation for the reactive mixture with 0.5% (by mole) H_2O doping.

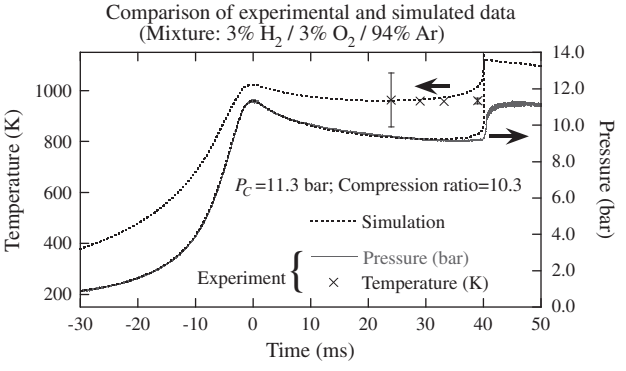

Fig. 6. Comparison of experimental pressure trace and temperature history with simulation for the reactive mixture without H_2O doping.

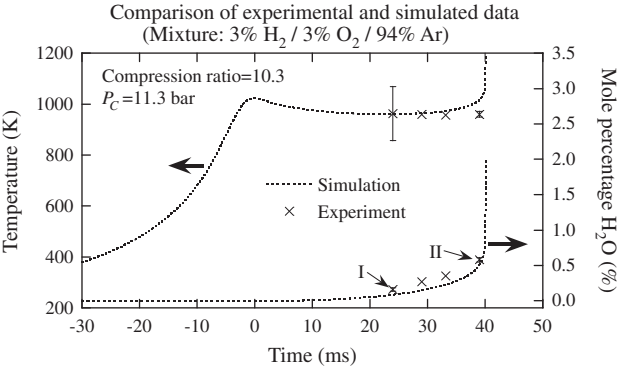

Fig. 7. Comparison of experimentally determined temperatures and water mole percentages with simulation for the reactive mixture without H_2O doping.

in the mixture before start of compression and remains almost constant till 14.1 ms after the end of compression. Beyond 14.1 ms the mole percentage of water in the mixture increases gradually to 1.14% just before ignition at 44.1 ms. Figure 5 also shows that the experimentally determined water level during the induction period is on an average slightly more than the simulated results. The simulated water mole percentage ranges from 95% of the experimentally determined water level at 24.1 ms to 76.3% at 44.1 ms. In Section 5.4, the uncertainty associated with the water concentration measurement will be discussed.

The experimentally determined temperatures and water mole percentages for the mixture without any initial water concentration are compared with the RCM simulation in Fig. 7. It is seen that no detectable water absorption signal is found before 24 ms after the end of compression. At 24 ms, the temperature determined is expected to have higher uncertainty due to low signal to noise ratio. Even though comparison of the experimental absorbance data and the best fit absorbance profile modeled using HITRAN leads to a temperature within −3 K of the RCM-simulated value, the uncertainty in temperature measurement owing to the noise in the experimental absorbance signal is as high as 11%. The normalized raw experimental absorbance data (gray symbols) with the corresponding HITRAN simulation (gray line) is shown for the same condition (data at 24 ms after the end of compression) in Fig. 8, demonstrating the quality of the experimental data and the comparison of the experimental and HITRAN-simulated absorbance data. It is noted that the "waves" seen in the absorbance profile are due to the etalon effects and are still significant even after accounting for the background signal containing etalon waves. For the subsequent points beyond 24 ms at which temperatures are determined experimentally, the signal to noise ratio improves due to increase in water concentration. The simulated temperature is found to be within +5 K of the experimental data for the next point (at 29 ms) during which the simulated and the experimental pressure traces are still close to each other. The difference between the simulated and experimentally determined temperatures increases to +14 K at 34 ms and +57 K at 39 ms. The reason for the increasing difference is evident from the comparison of the simulated and experimental pressure traces for this condition, as shown in Fig. 6. The simulated pressure trace indicates higher heat release in simulated data beyond 29 ms, thereby causing the simulated pressure trace to rise sharply above the experimental pressure trace. It can be noted from the raw absorbance data at 39 ms (black symbols in Fig. 8) that the signal to noise ratio improves substantially and the associated uncertainty in temperature measurement reduces to 1.2%.

Figure 7 also compares the experimentally determined water mole percentages with the RCM simulation. It is found that the measured mole percentages of water in the system are always slightly higher than the simulations. For this case, the simulated water level is 54.5% of the experimental data at 24 ms while at 39 ms it is 89.5% of the experimental data. It can also be noted that as it nears ignition, the rate of water production increases sharply in simulations as compared to the experimental data. The lowest water mole percentage for which reasonable absorbance data could be used is 0.16% at 24 ms after the end of compression. The measured water mole percentage increases to 0.58% just before ignition at 39 ms. As discussed earlier, the increase in water concentration leads to improvement in the signal to noise ratio thereby reducing the uncertainties of the temperature and water concentration measurements close to ignition. The improvement can be clearly noted from Fig. 8, showing comparison of the normalized raw absorbance data and the corresponding modeled absorbance using HITRAN for the data at 24 ms and the data at 39 ms after the end of compression.

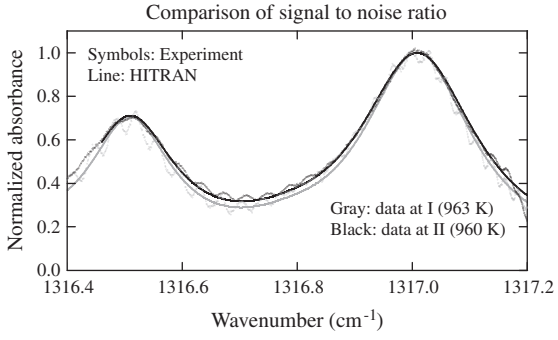

Fig. 8. Comparison of signal to noise ratio for two data points from Fig. 7 (I and II) showing improvement of signal to noise ratio close to ignition with higher water concentration.

It can, however, be noted that the overall match in ignition delay time is reasonably good for the two cases studied. Therefore, even when a global combustion characteristic is predicted well by a reaction mechanism, the evolution pathway might show some differences. This underscores the importance of this kind of *in situ* non-intrusive determination of temperature and species evolution profiles which can help us better understand the combustion kinetics of different fuels.

It was found in the previous study [12] that with single pass measurement, the mixture needed to be doped with about 2.87% H_2O for acceptable detection. In this study with the six-pass arrangement, reasonable signal with almost a sixth of that quantity in the mixture can be obtained. Therefore, even without any H_2O doping, the temperature prior to ignition could be successfully determined with very low H_2O concentration present in the mixture.

5.3. RCM core uniformity

The reaction inside the RCM reaction chamber progresses at high core temperatures. The progress of reaction in the thin thermal boundary layer is expected to be minimal (if no negative temperature coefficient response). Therefore, if the species (that we are measuring) boundary layer is to be considered, we can safely assume it to be thicker than or at least equal to the thermal boundary layer thickness.

Let us consider a situation where δ_T denotes the fraction of the thermal boundary layer thickness relative to the reaction chamber bore and δ_χ denotes the fraction of the species boundary layer thickness, as schematically shown in Fig. 9. It is to be noted from Fig. 9 that the species boundary layer covers the thermal boundary layer as well as a portion of the hot RCM core. The average values of temperature and water mole fraction (or number density) within the respective boundary layer are denoted by subscript *BL* and that for the core region is denoted by subscript *C*. The temperature and water mole fraction determined by comparing the experimental absorbance data with the HITRAN calculations are denoted as T_H and χ_H, respectively. Figure 9 schematically demonstrates the condition. The corresponding absorbance peak of a transition line can be written as:

$$\begin{aligned} A_{max} &= S_{T_H} N_H L \\ &= S_{T_{BL}} N_{BL} L \delta_T + S_{T_C} N_{BL} L (\delta_\chi - \delta_T) + S_{T_C} N_C L (1 - \delta_\chi) \end{aligned} \tag{8}$$

In Eq. (8), $S_T = \sum_i S^N_{v_i}(T) g_V(v_i - v_{max})$, which is evaluated at a temperature T and A_{max} occurs at v_{max}.

It can be noted that the first term on the right hand side (RHS) of Eq. (8) is for the zone within the temperature boundary layer δ_T which also includes a portion of the species boundary layer δ_χ, thus the temperature is T_{BL} and number density is N_{BL}. The second term on the RHS is for the zone within δ_χ but not covered by δ_T, and this

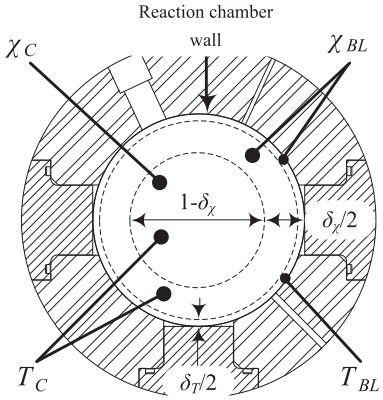

Fig. 9. RCM reaction chamber cross section with schematic representation of boundary layer zones and the corresponding temperatures and water mole fractions, with reference to Section 5.3.

zone covers a part of the hot core thus the temperature is T_C but the number density is N_{BL}. The third term on the RHS is for the hot core beyond the species boundary layer thus the temperature is T_C and the number density is N_C. Rewriting in terms of mole fraction, it yields:

$$S_{T_{BL}}\frac{P\chi_{BL}}{k_BT_{BL}}L\delta_T + S_{T_C}\frac{P\chi_{BL}}{k_BT_C}L(\delta_\chi-\delta_T) + S_{T_C}\frac{P\chi_C}{k_BT_C}L(1-\delta_\chi) = S_{T_H}\frac{P\chi_H}{k_BT_H}L \tag{9}$$

With further simplification, Eq. (9) can be written as:

$$\chi_H = \frac{T_H}{S_{T_H}}\left[S_{T_{BL}}\frac{\chi_{BL}}{T_{BL}}\delta_T + S_{T_C}\frac{\chi_{BL}}{T_C}(\delta_\chi-\delta_T) + S_{T_C}\frac{\chi_C}{T_C}(1-\delta_\chi)\right] \tag{10}$$

The finding of Mittal and Sung [17] has shown through planar laser-induced fluorescence experiments in RCM that the thermal boundary layer in the RCM with appropriately designed creviced piston is negligible ($\delta_T < 0.05$). A recent computational fluid dynamic study by Mittal et al. [27] demonstrated the effects of stroke and clearance on the core homogeneity, for various RCM operating conditions. The result therein showed that, for stroke length of 7″ and clearance of 0.55″ with N_2 bath gas, the core region was mostly homogeneous with very little boundary layer thickness for Crevice #0 in [27]. It was noted from [27] that the core homogeneity improves with increase in clearance. In this study (and [12]), the piston crevice dimension is the same as the dimension of Crevice #0 in [27], while the stroke length is 7″ and the clearance is 0.754″. Hence, the extent of core homogeneity in this study is supported by the computational fluid dynamic study of [27]. Analysis from the previous study [12] has further buttressed the insignificant thermal boundary layer effect for similar operating conditions even with Ar bath gas. Rewriting Eq. (10) with this approximation that δ_T is negligible and hence $T_H \approx T_C$ (also $S_{T_H} \approx S_{T_C}$), we get:

$$\chi_H = \chi_{BL}\delta_\chi + \chi_C(1-\delta_\chi) \tag{11}$$

Thus if there is any possible spatial variation in water number density due to differential water production within the hot core during the reactive run, this measurement technique only gives us the average water concentration along the line of sight. In addition, this technique is inadequate to determine any possible boundary thickness of the species of interest. However, any possible species boundary layer within the hot core does not affect the temperature measurement, since we are concerned only with the ratio of the two absorbance peaks.

5.4. Uncertainties in temperature and water concentration measurements

The error in the measured temperature, ΔT, using the ratio of the chosen line pair, R, has been discussed in [12] and is given by:

$$\Delta T \sim \frac{\Delta R}{dR/dT} \tag{12}$$

where ΔR is the error in the ratio. The change of the peak ratio with temperature T, dR/dT, is calculated using HITRAN with updated broadening parameters. Recognizing that the uncertainty in peak ratio comparison, $\mathcal{U}_R$, is contributed mainly by the uncertainty in line strengths as well as the uncertainty in the peak height determination [12], ΔR is the product of $\mathcal{U}_R$ with the line ratio and can be expressed as:

$$\Delta R = R\mathcal{U}_R = R\sqrt{\mathcal{U}^2_{S_{v1}} + \mathcal{U}^2_{S_{v2}} + \mathcal{U}^2_{A_{1max}} + \mathcal{U}^2_{A_{2max}}} \tag{13}$$

where $\mathcal{U}$ denotes the uncertainty for the corresponding subscripts. The maximum heights of the first and second peaks are respectively denoted by A_{1max} and A_{2max}, and S_{v1} and S_{v2} are the calculated line strengths of the first and second lines, respectively. In the previous study [12], it was estimated that the uncertainty involved in temperature measurements for the temperature window of 550–1300 K is in the range of ±0.6–1.6%. However, it should be noted that the water addition in [12] was sufficient to get a very good signal to noise ratio, and hence the uncertainties in A_{1max} and A_{2max} were much less.

For the case with water doping in this study, the absorption path length is increased by six times whereas the initial water concentration is less by almost a factor of six. Thus, the resultant uncertainty in peak heights is ~1%, which is about the same as that in [12]. As such, the uncertainty expected in the temperature determination for the water doping case is comparable to [12]. When we estimate the uncertainty for the case without water addition, for the worst case situation corresponding to point 'I' in Fig. 7, the water mole percentage is very less (0.16%), thereby lower signal to noise ratio. Since the uncertainty in peak heights is ~10% (cf. Fig. 8), this leads to a temperature uncertainty of ~11%. However, for the point just before ignition, i.e. point 'II' denoted in Fig. 7, the water concentration is higher leading to much better signal to noise ratio. The temperature uncertainty based on this improved signal to noise ratio at point 'II' is estimated to be 1.2%.

Following the methodology of [12], uncertainty analysis for the species concentration measurement is discussed as follows. The mole fraction χ of the species of interest is given by

$$\chi = \frac{Nk_BT}{P} \tag{14}$$

Substituting the expression for the number density, $N = \frac{A_{max}}{S_TL}$, in Eq. (14), we get

$$\chi = \left(\frac{A_{max}}{S_TL}\right)\left(\frac{k_BT}{P}\right) \tag{15}$$

Thus using the propagation of error method [28], the uncertainty in mole fraction is expressed as:

$$\mathcal{U}_\chi = \sqrt{\mathcal{U}^2_{A_{max}} + \mathcal{U}^2_T + \mathcal{U}^2_{S_T} + \mathcal{U}^2_L + \mathcal{U}^2_P} \tag{16}$$

For the worst case situation corresponding to the data at 24 ms for the case without water addition, i.e. point 'I' in Fig. 7 with 0.16% water, the uncertainty in mole fraction $\mathcal{U}_\chi$ is mainly dominated by the large uncertainty in the absorbance signal $\mathcal{U}_{A_{max}}$ (~10%) due to the noise in the raw signal as well as the uncertainty in the corresponding temperature measurement $\mathcal{U}_T$ (~11%). Even if we consider uncertainty in path length of $\mathcal{U}_L < 5\%$, allowing for the 5% thermal

boundary layer, taking $\mathcal{U}_{S_T} < 0.83\%$ (approximating with the maximum uncertainty in the line strength of the transition lines considered [12]), and $\mathcal{U}_P < 0.4\%$, the uncertainty in determination of H_2O mole fraction is $\mathcal{U}_\chi < 15.7\%$. Similar calculation done for the data at 39 ms for the case without water addition, namely point 'II' in Fig. 7 with 0.58% water, leads to an uncertainty of $\mathcal{U}_\chi < 5.3\%$. Furthermore, the uncertainties in water concentration measurements for the case with 0.5% water addition are found to be between 5.2% and 6.1% due to less noise in the absorbance signal. It is to be noted that in this uncertainty analysis, a very conservative value for the uncertainty in path length is used. It is also worthy to mention that within the spectral scan range (1316.4–1317.8 cm^{-1}), the experimental absorbance profile is matched with the HITRAN model to determine the peak height. Therefore, inclusion of uncertainties from the line shape factors will contribute to undue overestimation of the temperature uncertainty; hence the line shape factor uncertainty is not included in the uncertainty calculations.

6. Concluding remarks

Quantum cascade laser in the mid-IR region is used for determining the collisional broadening parameters of the water transition lines in the range of 1316.4–1317.8 cm^{-1} with H_2 or O_2 as a bath gas. A six-pass custom built Herriott cell is used in the calibration experiments. Line broadening coefficient γ_0 for the H_2O transition lines in H_2 ranges from 0.0229 to 0.0752 cm^{-1}/atm whereas the temperature exponent n varies from −0.29 to 1.17. The γ_0 values for the H_2O transition lines in O_2 are from 0.0046 to 0.0272 cm^{-1}/atm and the n values are found to be from −0.24 to 0.55.

The Quantum cascade laser in the mid-IR region is further used for absorption spectroscopy in this study to measure the time histories of temperature and water concentration inside a RCM. The line broadening parameters of H_2O transition lines in H_2 or O_2 as a bath gas determined in this study as well as those determined in Ar bath gas in the previous study [12] are utilized for the temperature and species concentration measurements. A six-pass absorption setup is implemented in the RCM to detect very low concentration of water. Temperatures are determined experimentally for reactive mixtures with and without H_2O doping. The temperatures obtained from the RCM simulations are within ±5 K of the experimentally determined temperatures for most of the cases when the simulated and experimental pressure traces are in agreement. Deviation of simulated temperatures from experimentally determined temperatures are noted for conditions when there is notable difference in the pressure traces due to the discrepancy in the experimental and simulated ignition delays. The water mole percentages determined from absolute absorbance values lead to results slightly higher than the simulated data till just before ignition. The rate of water production close to ignition is noted to be faster for the simulation when compared to the experimental data, which is mainly because of the mismatch in ignition delay prediction. It is demonstrated that even with very dilute H_2/O_2 mixture, which produces low concentration of water during the induction period, the current setup is still able to get good signal and measure the temperature just before ignition. With the experience gained from this study, we estimate that richer H_2/O_2 mixtures in argon can be measured till end of compression pressure of P_C = 15–17 bar. Most of the other auto-ignitable mixtures in RCM are expected to produce more H_2O during the induction period, thus indicating that even without water doping, temperatures for reactive mixtures can be measured prior to ignition.

An uncertainty analysis for temperature and water concentration measurements is also conducted. For the condition with no water doping, the uncertainties in temperature and water mole fraction measurements are 11% and 15.7%, respectively, for the worst case scenario (with 0.16% water present in the system), while for the best condition they are respectively 1.2% and 5.3% (when 0.58% water is present in the system). In general, the uncertainty in water mole fraction measurement for the case with 0.5% water doping is within 5.2–6.1%. It is further noted that the uncertainty analysis for water mole fraction measurement is carried out with a very conservative estimate for the uncertainty of the path length (5%).

Acknowledgments

This material is based upon work supported as part of the Combustion Energy Frontier Research Center, an Energy Frontier Research Center funded by the U.S. Department of Energy, Office of Science, Office of Basic Energy Sciences, under Award Number DE-SC0001198.

References

[1] G. Wysocki, R. Lewicki, R.F. Curl, F.K. Tittel, L. Diehl, F. Capasso, M. Troccoli, G. Hofler, D. Bour, S. Corzine, R. Maulini, M. Giovannini, J. Faist, Appl. Phys. B: Lasers Opt. 92 (2008) 305–311.
[2] B.W.M. Moeskops, H. Naus, S.M. Cristescu, F.J.M. Harren, Appl. Phys. B: Lasers Opt. 82 (2006) 649–654.
[3] M. Brandstetter, B. Lendl, Sens. Actuators, B 2011. doi:10.1016/j.snb.2011.06.081.
[4] C. Young, S.-S. Kim, Y. Luzinova, M. Weida, D. Arnone, E. Takeuchi, T. Day, B. Mizaikoff, Sens. Actuators, B 140 (2009) 24–28.
[5] V.L. Kasyutich, P.A. Martin, Sens. Actuators, B 157 (2011) 635–640.
[6] L. Li, F. Cao, Y. Wang, M. Cong, L. Li, Y. An, Z. Song, S. Guo, F. Liu, L. Wang, Sens. Actuators, B 142 (2009) 33–38.
[7] B.W.M. Moeskops, S.M. Cristescu, F.J.M. Harren, Opt. Lett. 31 (2006) 823–825.
[8] A. Elia, C.D. Franco, V. Spagnolo, P.M. Lugarà, G. Scamarcio, Sensors 9 (2009) 2697–2705.
[9] J.B. McManus, J.H. Shorter, D.D. Nelson, M.S. Zahniser, D.E. Glenn, R.M. McGovern, Appl. Phys. B: Lasers Opt. 92 (2008) 387–392.
[10] J. Vanderover, M.A. Oehlschlaeger, Appl. Phys. B: Lasers Opt. 99 (2010) 353–362.
[11] X. Chao, J.B. Jeffries, R.K. Hanson, Proc. Combust. Inst. 33 (2011) 725–733.
[12] M. Uddi, A.K. Das, C.J. Sung, Appl. Opt. Available online: <http://8.18.37.105/ao/upcoming_pdf.cfm?id=164635>.
[13] A. Farooq, J.B. Jeffries, R.K. Hanson, Meas. Sci. Technol. 19 (2008) 075604.
[14] L.S. Rothman, I.E. Gordon, R.J. Barber, H. Dothe, R.R. Gamache, A. Goldman, V.I. Perevalov, S.A. Tashkun, J. Tennyson, J. Quant. Spectrosc. Radiat. Transfer 111 (2010) 2139–2150.
[15] J. Fischer, R.R. Gamache, A. Goldman, L.S. Rothman, A. Perrin, J. Quant. Spectrosc. Radiat. Transfer 82 (2003) 401–412.
[16] A.K. Das, C.J. Sung, Y. Zhang, G. Mittal, Int. J. Hydrogen Energy 37 (2012) 6901–6911.
[17] G. Mittal, C.J. Sung, Combust. Sci. Technol. 179 (2007) 497–530.
[18] G. Mittal, C.J. Sung, Combust. Flame 145 (2006) 160–180.
[19] D. Herriott, H. Kogelnik, R. Kompfner, Appl. Opt. 3 (1964) 523–526.
[20] A.E. Lutz, R.J. Kee, J.A. Miller, Sandia Report No. SAND 87–8248, Sandia National Laboratories, 1998.
[21] Z. Hong, D.F. Davidson, R.K. Hanson, Combust. Flame 158 (2011) 633–644.
[22] R.J. Kee, F.M. Rupley, J.A. Miller, Sandia Report No. SAND 89–8009, Sandia National Laboratories, 1989.
[23] R.A. Toth, L.R. Brown, J. Mol. Spectrosc. 218 (2003) 135–150.
[24] L.R. Brown, C. Plymate, J. Quant. Spectrosc. Radiat. Transfer 56 (1996) 263–282.
[25] T.M. Goyette, D.W. Ferguson, F.C. DeLucia, J.M. Dutta, C.R. Jones, J. Mol. Spectrosc. 162 (1993) 366–374.
[26] S. Langlois, T.P. Birbeck, R.K. Hanson, J. Mol. Spectrosc. 167 (1994) 272–281.
[27] G. Mittal, M.P. Raju, C.J. Sung, Fuel 94 (2012) 409–417.
[28] H.W. Coleman, W.G. Steele Jr., Experimentation and Uncertainty Analysis for Engineers, John-Wiley & Sons, 1989.